INTERNATIONAL JOURNAL FOR NUMERICAL AND ANALYTICAL METHODS IN GEOMECHANICS
Int. J. Numer. Anal. Meth. Geomech., **23**, 1–21 (1999)

NON-LOCAL EFFECTS ON DYNAMIC DAMAGE ACCUMULATION IN BRITTLE SOLIDS

E. P. CHEN*

Structural and Thermomechanical Modeling Department, Sandia National Laboratories, Livermore, CA 94551-0969, U.S.A.

SUMMARY

This paper presents a non-local analysis of the dynamic damage accumulation processes in brittle solids. A non-local formulation of a microcrack-based continuum damage model is developed and implemented into a transient dynamic finite element computer code. The code is then applied to the study of the damage accumulation process in a concrete plate with a central hole and subjected to the action of a step tensile pulse applied at opposite edges of the plate. Several finite element discretizations are used to examine the mesh size effect. Comparisons between calculated results based on local and non-local formulations are made and non-local effects are discussed. Copyright © 1999 John Wiley & Sons, Ltd.

Key words: damage; nonlocal; dynamic; continuum; numerical; brittle solid

INTRODUCTION

Continuous demands on safety and efficient design have placed increasing emphasis on fracture and failure analyses of engineering materials and structures. Continuum damage mechanics have been applied to study the phenomenon of brittle fracture in solids under dynamic loads with varying degrees of success.[1–6] Because of the complex geometries and loading conditions involved, numerical simulation techniques have become the tools of choice. Two common problems associated with damage analyses by classical continuum damage mechanics are softening and localization. The consequences of failing to take into account these two problems properly usually manifested in solutions which are dependent on the discretizaton size. A potential remedy is to cast the field equations in a non-local setting such that the high gradients associated with the field parameters in these problems can be captured. The non-locality is usually represented by an internal length scale which can be introduced in formulations ranging from the Cosserat and micropolar theories,[7,8] the gradient theory,[9,10] fully non-local[11] and partially non-local[12,13] representations. An alternative approach based on the disturbed state concept has also been proposed by Desai *et al.*[14,15] to alleviate mesh-size dependence and provide consistent localization results.

The purpose of this research is to investigate the appropriateness of applying non-local damage models to analyse dynamic brittle fracture. The study is based on the comparisons between

*Correspondence to: E. P. Chen, Structural and Thermomechanical Modeling Department, Sandia National Laboratories, Livermore, CA 94551-0969, U.S.A.

Contract grant sponsor: U.S. Department of Energy; contract grant number: DE-AC04-94AL85000

CCC 0363–9061/99/010001–21$17.50

Received 15 January 1996
Revised 22 January 1997

numerical results obtained from the same damage model with both a non-local and a local formulation. The damage model selected is the one developed by the author and his coworkers[1–6] to simulate brittle rock fracturing. A non-local version is developed here by utilizing the non-local formulation suggested in Reference 13 in which non-locality is only applied to those internal state variables involved with material damage. The model has been implemented into the transient finite element code PRONTO 2D[16] for numerical analysis. An example problem has been defined and results have been obtained from both local and non-local calculations. To examine mesh size effect, several discretizations are used in the numerical computations. Comparisons between these results have been made. Based on these findings, it is clear that mesh-size dependence can be alleviated by adopting a non-local damage model formulation. However, the determination of the internal length scale associated with the non-local formulation is certainly non-trivial. Moreover, non-locality tends to smear out localized deformations and thus may suppress truly local failure modes. This may render the non-local models inappropriate for predicting localized failure mechanisms.

CONTINUUM DAMAGE MODEL DESCRIPTION

The basic assumption of the damage model is that the material is permeated by an array of randomly distributed cracks which grow and interact with one another under tensile loading. The model does not attempt to treat each individual crack, but rather treats the growth and interaction of cracks as internal state variables which represent damage accumulation in the material. The damage is reflected in the degradation of the material stiffness following the equations derived by Budiansky and O'Connell[17] for a random array of penny-shaped cracks in an isotropic elastic medium:

$$\frac{\bar{K}}{K} = 1 - \frac{16}{9}\left(\frac{1-\bar{\nu}^2}{1-2\bar{\nu}}\right) C_{\mathrm{d}} \tag{1}$$

$$\frac{\bar{G}}{G} = 1 - \frac{32}{45}\frac{(1-\bar{\nu})(5-\bar{\nu})}{(2-\bar{\nu})} C_{\mathrm{d}} \tag{2}$$

$$\frac{\bar{E}}{E} = 1 - \frac{16}{45}\frac{(1-\bar{\nu}^2)(10-3\bar{\nu})}{(2-\bar{\nu})} C_{\mathrm{d}} \tag{3}$$

where K, G, E and ν are material bulk modulus, shear modulus, Young's modulus and Poisson's ratio, respectively. Barred quantities such as $\bar{K}$ represent degraded properties and C_{d} is the crack density parameter. Additionally, the crack density parameter is related to the virgin and damaged Poisson's ratio through

$$C_{\mathrm{d}} = \frac{45}{16}\frac{(\nu-\bar{\nu})(2-\bar{\nu})}{(1-\bar{\nu}^2)[10\nu-\bar{\nu}(1+3\nu)]} \tag{4}$$

The damage variable is defined as

$$D = \frac{16}{9}\left(\frac{1-\bar{\nu}^2}{1-2\bar{\nu}}\right) C_{\mathrm{d}} \tag{5}$$

such that $\bar{K} = K(1 - D)$. The crack density parameter is assumed to be proportional to the product of N, the number of cracks per unit volume, and a^3, the cube of the average crack dimension in a representative volume. Following Grady and Kipp,[18] N is expressed as a Weibull statistical distribution function activated by the bulk strain measure $\varepsilon_v = (\varepsilon_x + \varepsilon_y + \varepsilon_z)/3$, according to

$$N = k(\varepsilon_v)^m \tag{6}$$

in which k and m are material constants to be determined from strain-rate-dependent tensile fracture stress data. The average crack dimension a is estimated from the nominal fragment diameter for dynamic fragmentation in a brittle material[19] as

$$2a = \left(\frac{\sqrt{20}K_{\mathrm{IC}}}{\rho C\dot{\varepsilon}_{v\max}}\right)^{2/3} \tag{7}$$

where ρ is the mass density, C is the uniaxial wave speed $(E/\rho)^{1/2}$, and K_{IC} is the fracture toughness of the material. Also, $\dot{\varepsilon}_{v\max}$ is the maximum volumetric strain rate experienced by the representative volume element for the entire loading process. Equations (1)–(5) can also be cast into rate form to relate stress and strain rates. When bulk tension occurs in the material, it is possible to calculate, at each time step, the crack density parameter C_{d} by making use of equations (6) and (7) and then damage parameter D through equation (5). The material stiffness is then degraded according to equations (1)–(5). In compression, the material behaves as an elastic/perfectly plastic solid. Details of the model development are given in Reference 1 and will not be repeated here.

Modifications have been made to the above model to render it a more versatile tool. Because the equations derived by Budiansky and O'Connell[17] are limited to dilute crack concentrations, the crack density parameter has a limiting value of 9/16. To extend the range of crack densities, an expression[20]

$$\bar{\nu} = \nu \mathrm{e}^{-(16/9)\beta C_{\mathrm{d}}}, \quad 0 \leqslant \beta \leqslant 1 \tag{8}$$

was used to approximate equation (4). Equation (8) recovers Budiansky and O'Connell's expression for dilute crack concentrations at small crack density C_{d} and attains the correct limit of zero stiffness for large C_{d} values. In comparison with the expression in Reference 1, the crack density parameter $16C_{\mathrm{d}}/9$ is effectively replaced by $1 - \mathrm{e}^{-(16/9)\beta C_{\mathrm{d}}}$. The value of β controls the unloading and reloading behaviour and relaxes the restriction of elastic unloading in the original model.

For many brittle solids, pressure-dependent inelastic response under compressive loads is observed. An improvement is made by extending the elastic/perfectly plastic compressive response to one that employs a Drucker–Prager yield surface[21]:

$$\bar{F} = \bar{\sigma}^2 - (c_1 + c_2 P)^2 = 0 \tag{9}$$

with $\bar{\sigma}$ the effective stress, P the mean stress and c_1 and c_2 material constants determined from experimental data. To avoid too much dilation, a von Mises flow rule of the type

$$\dot{\varepsilon}^{\mathrm{p}}_{ij} = \dot{\lambda}\frac{s_{ij}}{\sqrt{s_{ij}s_{ij}}} \tag{10}$$

is adopted. In equation (10), $\dot{\varepsilon}^{\mathrm{p}}_{ij}$ is the plastic strain rate tensor, $\dot{\lambda}$ is the plastic loading rate parameter, and s_{ij} is the deviatoric stress tensor.

CHARACTERISTICS OF THE DAMAGE MODEL

Characteristics of the continuum damage model described are examined here for the same oil shale as in Reference 1. Nominal material properties such as the mass density, the Young's modulus, the Poisson's ratio and the fracture toughness are taken to be 2270 g/m^3, 10·8 GPa, 0·2 and 1·0 MPa m$^{1/2}$, respectively. Shear strength τ was approximated by a linear relationship of $\tau = 200{\cdot}0 + 0{\cdot}5\,\mathrm{P}$ (MPa). Strain-rate-dependent tensile fracture stress data are required to determine the constants k and m in equation (6). *In lieu* of measured data, it is possible to estimate this dependence using an expression derived in Reference 22 for the tensile fracture stress σ_c:

$$\sigma_c = \left(\frac{9\pi E K_{IC}^2}{16 N_s^2 C_s}\right)^{1/3} \dot{\varepsilon}^{1/3} \tag{11}$$

where N_s is a shape factor (1·12 for penny-shaped cracks) and C_s is the shear wave velocity of the material. Thus, k and m are really not additional material constants for the model. For the oil shale, Kipp and Grady[23] reported fracture stress versus strain rate data and this is shown in Figure 1. Based on these data and the material properties given above, m and k are determined to be 7·0 and $5{\cdot}116 \times 10^{22}$/m^3, respectively.

Using these material properties and 0·5 for β, the response of the oil shale under bulk tension can now be examined. Figure 2 shows the pressure–volumetric strain relationship under uniaxial homogeneous straining for three strain rates. In this figure, positive pressure denotes bulk tension. Strain softening is observed as a consequence of the micro-cracking damage accumulation. The material's capability to carry bulk tension increases with the strain rate. Damage accumulation as a function of volumetric strain is shown in Figure 3. The loading/unloading/reloading behaviour for 1000/s strain rate is exhibited in Figures 4 and 5 in terms of the pressure- and damage-volumetric strain plot, respectively. It is seen that the damage evolution is an irreversible process. During reloading, no more damage accumulation will take place until the strain level has exceeded the previous maximum. The value for β controls the unloading response. For $\beta = 0$, elastic unloading along the damaged bulk modulus will result. For $\beta = 1$, unloading is

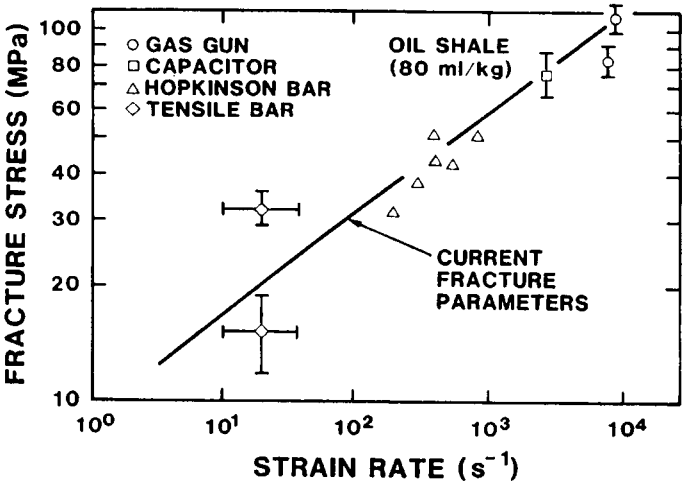

Figure 1. Oil Shale tensile fracture stress versus strain rate data

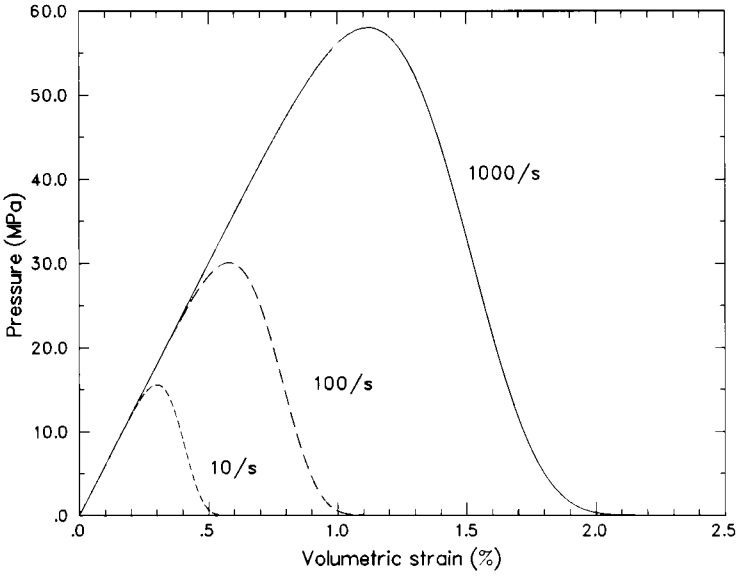

Figure 2. Oil Shale bulk response under tension

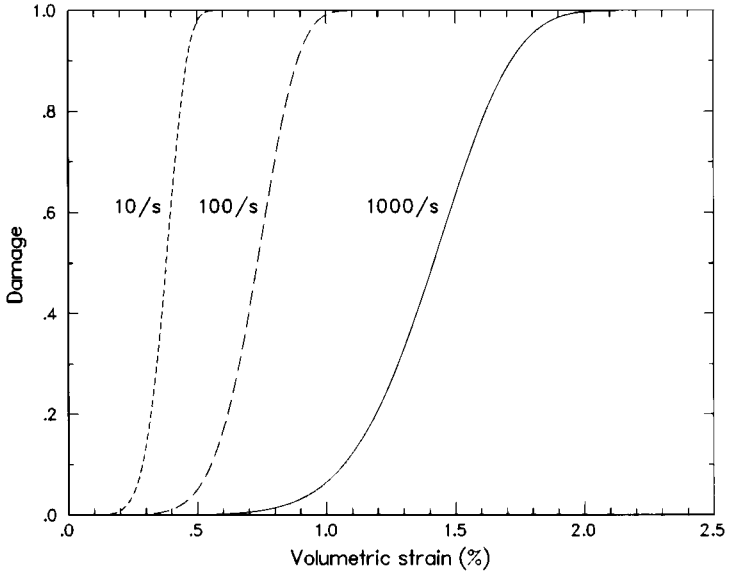

Figure 3. Damage versus volumetric strain plot

along the original bulk modulus similar to elastic/plastic behaviour. For β between 0 and 1, a combined damage/plastic unloading response results. The effect of β is illustrated in Figure 6. Note that because of the modifications, the numerical values reported here are slightly different from those in Reference 1. Also, the exponential representation in equation (8) renders better numerical convergence and smooth softening responses.

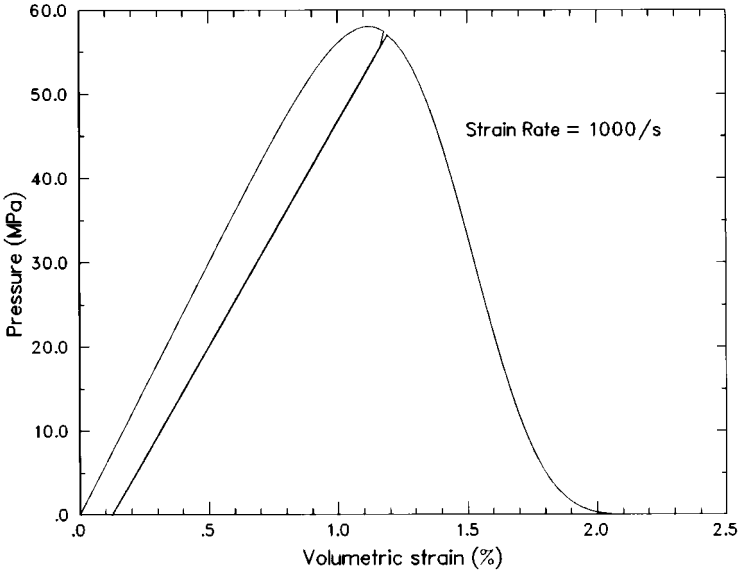

Figure 4. Cyclic bulk tension response of Oil Shale

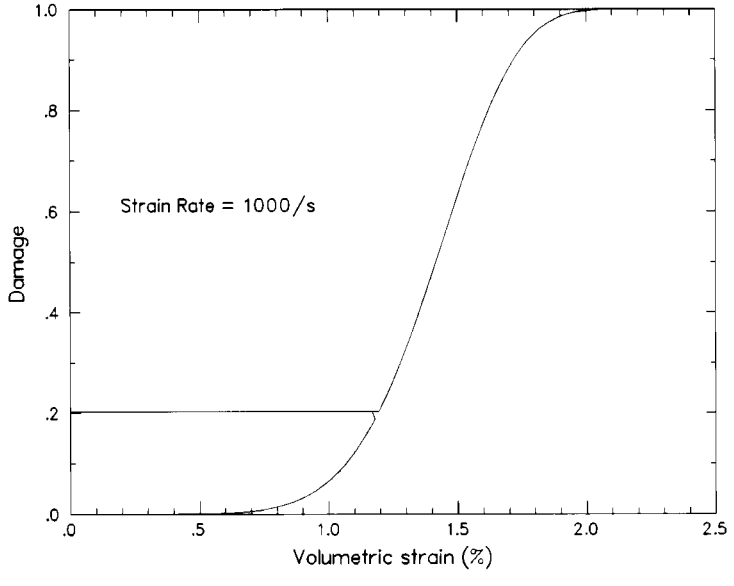

Figure 5. Cyclic damage behaviour

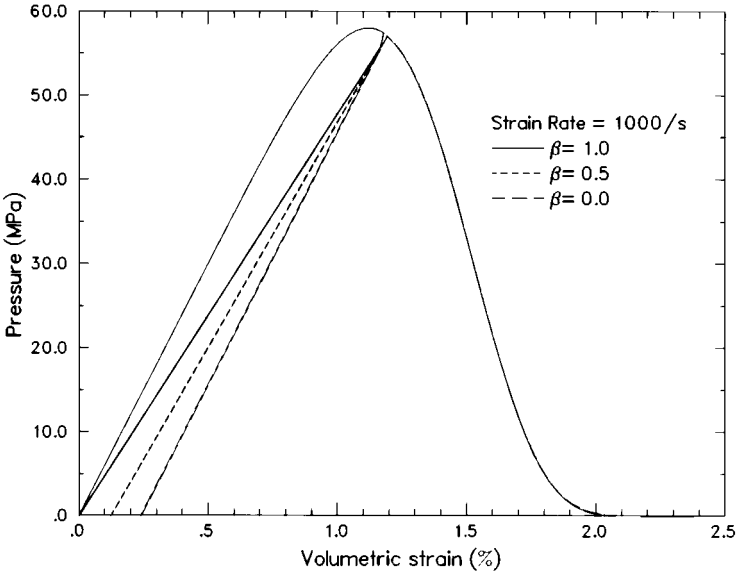

Figure 6. Effect of β on unloading

NON-LOCAL FORMULATION

Non-local formulations involve the introduction of localization limiters, usually an internal length scale, into classical continuum field equations. Depending on the degree of sophistication, several theories exist in the literature.[7–13,24] The purpose of the present investigation is to examine general non-local effects and it suffices to consider a simple yet efficient formulation. To this end, the non-local continuum with local strain model[13] is adopted here. Typically, for this model, some of the variables in the constitutive equation are defined by spatial averaging while the others retain their local definitions. The spatial average of the magnitude of an arbitrary variable γ at location $\mathbf{x}$ may be defined by the equation

$$\langle \gamma(\mathbf{x}) \rangle = \frac{1}{V_r(\mathbf{x})} \int_V \alpha(\mathbf{s} - \mathbf{x}) \gamma(\mathbf{s}) \, \mathrm{d}V \tag{12}$$

in which

$$V_r(\mathbf{x}) = \int_V \alpha(\mathbf{s} - \mathbf{x}) \, \mathrm{d}V \tag{13}$$

The pointed brackets $\langle \, \rangle$ denote the averaging operator, V is the volume of the body, $\alpha(\mathbf{x})$ is the weighing function which defines the averaging, and $\mathbf{s}$ is the general co-ordinate vector. The selection of the weighing function should be based on physical considerations. The normal (Gaussian) distribution function (error density function)

$$\alpha(x) = \mathrm{e}^{-|x|^2/4l^2} \tag{14}$$

was selected in Reference 13 for two-dimensional geometries. In equation (14), l is the characteristic length which is a material property that defines the diameter of the representative volume.

Judicious choices of the variables which should be subjected to spatial averaging are required. In Reference 13, for a non-local plasticity model, only the plastic strain was subjected to spatial averaging and satisfactory results were obtained. Motivated by the results in Reference 13, the present non-local formulation will apply spatial averaging to state variables relating to material damage while others maintain their local definitions. By analysing equations (1)–(8) and replacing the crack density parameter $16C_d/9$ with $1 - e^{-(16/9)\beta C_d}$, a mixed system of algebraic and ordinary differential equations can be constructed for the evolution of tensile damage as follows:

$$\dot{C}_d = \frac{5km\varepsilon_v^{m-1}}{2}\left(\frac{K_{IC}}{\rho C\dot{\varepsilon}_{v\,max}}\right)^2 \dot{\varepsilon}_v \tag{15}$$

$$D = \frac{1-\bar{v}^2}{1-2\bar{v}}\left(1 - e^{-(16/9)\beta C_d}\right) \tag{16}$$

$$\bar{K} = K(1-D) \tag{17}$$

$$\bar{G} = G\left[1 - \frac{2}{5}\frac{(1-\bar{v})(5-\bar{v})}{(2-\bar{v})}(1 - e^{-(16/9)\beta C_d})\right] \tag{18}$$

$$\dot{P} = 3\bar{K}\dot{\varepsilon}_v - eK\varepsilon_v\dot{D} \tag{19}$$

$$\dot{s}_{ij} = 2\bar{G}\dot{e}_{ij} + 2\dot{\bar{G}}e_{ij} \tag{20}$$

where s_{ij} and e_{ij} are the deviatoric stress and strain tensor, respectively, and the dot superscript denotes differentiation with respect to time. Together with equation (8), equations (15)–(20) can be used to calculate the evolution of tensile damage in the material. For the given imposed state of deformation in a time or loading step, the crack density increment is calculated from equation (15) and C_d is updated to the end of the time step. The damage increment is obtained by differentiating equation (16) and its value can be updated. It follows from equations (8), (17) and (18) that the time rate and the degraded Poisson's ratio, bulk and shear modulus can be evaluated. Then, through equations (19) and (20), the stress state is obtained. In compression, local plasticity theory of the Prager–Drucker type governs the constitutive behaviour of the material.

In the non-local formulation, equation (15) is used to update the crack density increment and crack density for every element in a given time step, just like the local calculations. However, before proceeding to evaluate equations (16)–(20), the averaging operator based on equations (12)–(14) and the characteristic length l is applied to C_d to obtain $\langle C_d\rangle$ for every element. This is done by approximating the integrals in equations (12) and (13) with summations over all elements in the same material block, i.e. the $\langle C_d\rangle$ value at ith element is evaluated through

$$\langle C_d\rangle = \frac{1}{A}\sum_j e^{|\mathbf{x}|^2/4l^2} A_j (C_d)_j \tag{21}$$

where A is the total area $A = \sum_j A_j$ and the distance $\mathbf{x} = \mathbf{x}_j - \mathbf{x}_i$ in equation (21) is measured between element integration points. This $\langle C_d\rangle$ value is used in equation (16) to evaluate $\langle D\rangle$. The $\langle C_d\rangle$ and $\langle D\rangle$ are then inserted in equations (17)–(20) to update the degraded stiffness and stress

state in all elements. Alternatively, the summation in equation (21) can be approximated to include only elements within a certain distance from the element in question. For the present example problems, the added computation costs by carrying all elements are insignificant. Consequently, equation (21) is used. Without going into more details, this non-local damage model have been vectorized and implemented into the explicit finite element code PRONTO 2D[16] for efficient computations.

NUMERICAL CALCULATIONS

General non-local effects are examined based on the comparisons of results between local and non-local calculations. The example problem selected is the same one used in Reference 6 which involves the sudden stretching of a plate with a centrally located hole. Consider the $0{\cdot}2\,\mathrm{m} \times 0{\cdot}4\,\mathrm{m}$ rectangular plate with a $0{\cdot}1\,\mathrm{m}$ diameter hole in the centre in Figure 7. A step tensile pulse is applied symmetrically to the left and right edge of the plate. The plate consists of the same Oil Shale material as the one given in the section on the characteristics of the damage model. For numerical calculations, the pulse is given a strength of $10{\cdot}0\,\mathrm{MPa}$. Both the non-local and local damage models as implemented in the finite element code PRONTO 2D are used to obtain the dynamic response of the plate. The plane strain condition is assumed to prevail. Because of symmetry, only one-quarter of the geometry in Figure 7 needs to be included in the finite elements mesh. Four meshes with varying degree of fineness are chosen to investigate mesh size effects. Figure 8 shows the most coarse mesh with 75 elements and 96 nodes. A 90° rotation of the schematic drawing in Figure 7 has been made. The boundary of the hole is divided into 10 elements. The second mesh is constructed by simply doubling the numbers of divisions in both the x and y directions in Figure 8. Thus, the mesh consists of 300 elements and 341 nodes. In a similar expansion, the third mesh is constructed with 1200 elements and 1281 nodes. To avoid an excessive number of elements, the fourth mesh only doubles the number of divisions in the third mesh in the lower right part of the plate and consists of 2800 elements and 2921 nodes. This is justified because with the applied tensile pulse, the high stress gradients are anticipated to concentrate around the lower right part of the plate and it is not necessary to place fine mesh in other parts of the plate. The finest mesh with 2800 elements is shown in Figure 9.

Calculations were carried out on the Cray YMP computer at Sandia National Laboratories. the results of the local continuum model are presented first. The evolution of damage focused on

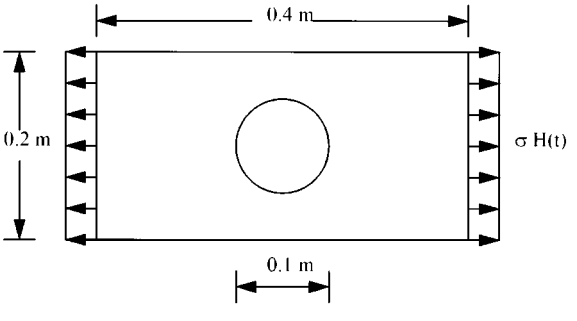

Figure 7. Schematic drawing of the example problem

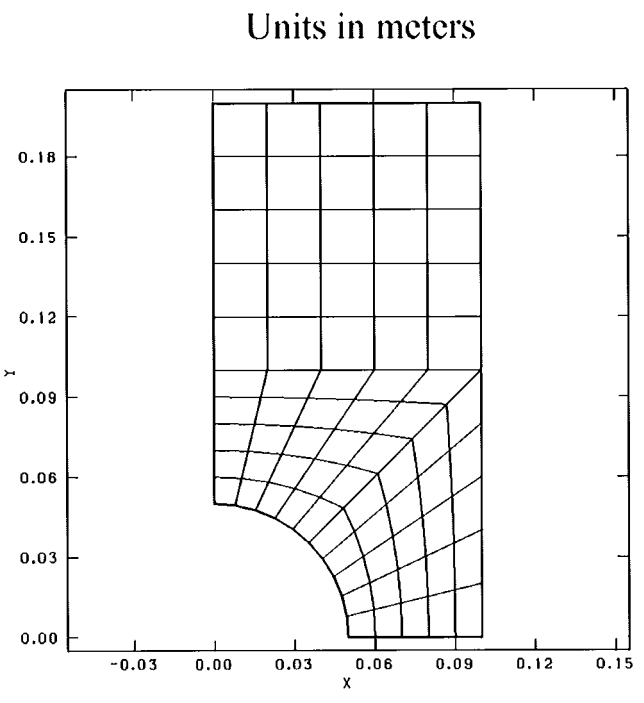

Figure 8. Finite element mesh with 75 elements

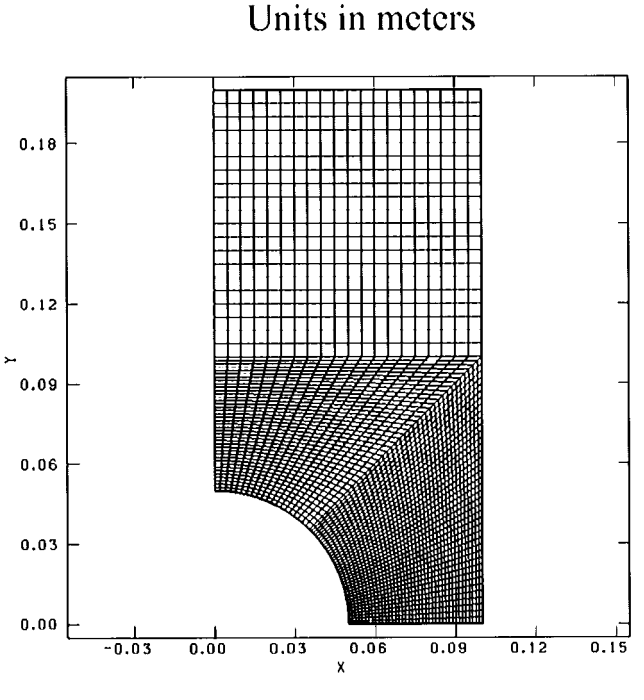

Figure 9. Finest mesh with 2800 elements

the lower $0{\cdot}09 \times 0{\cdot}09$ m area of the plate is depicted at four time intervals at 0·175, 0·2, 0·215 and 0·225 ms after the tensile pulse has been applied. The results are given in Figure 10–13, respectively, corresponding to the four meshes. It is clear that damage localizes near the lower right edge of the hole and with more refined mesh, damage localizes into a narrower band. The fact that damage occurs at a direction deviating from the bottom edge of the hole is due to the effect of wave propagation and the strain rate dependence of the damage model. A more detailed explanation is given in Reference 6 and will not be repeated here.

The localization of deformation can also be observed by plotting the distribution of bulk strain around the boundary of the hole. These are shown in Figures 14–17 for the four meshes at four time intervals. Because the actions are concentrated at the lower right part of the plate, only the lower 45° arc of the hole boundary has been included. The bulk strains are the values at integration points of the first layer of elements closest to the hole boundary. The distance is measured counterclockwise from the bottom edge of the hole. Bulk strain localization is clearly observed. Also, the results do not converge with mesh refinement in that the peak strain localizes into a narrower band and attains larger values with mesh refinement.

An additional parameter, namely the characteristic length, is required for the non-local calculations. For the present model, the localization limiter is taken to be the radius of the minimum crack that will be activated during the loading process. From the local calculation, the nominal strain rate attained under the applied tensile pulse is approximately 1000/s. Thus, from equation (7), the minimum crack radius can be calculated and the value is 0·0005 m. This value is used for the characteristic length l in equation (14). This value compares to the minimum dimensions of 0·0196, 0·0098, 0·00196, and 0·00098 m, respectively, for the four meshes selected in the calculations.

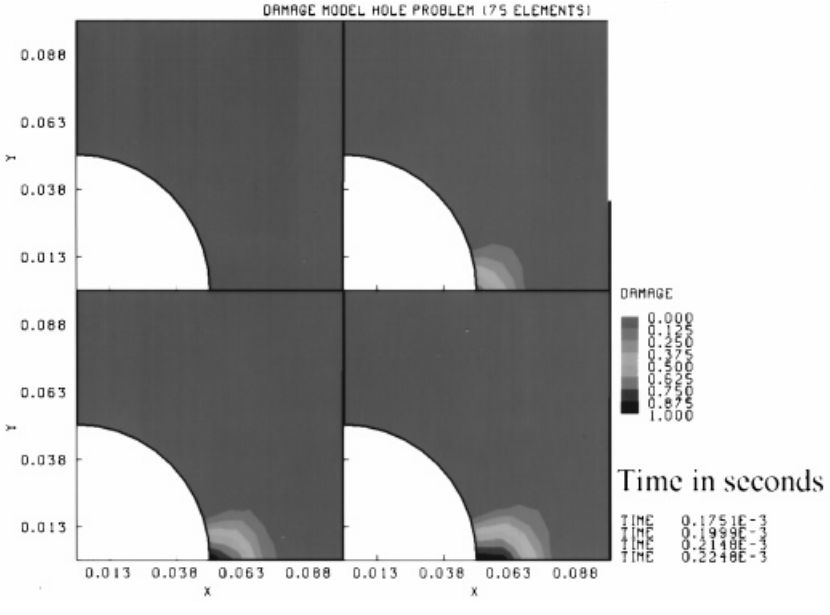

Figure 10. Damage evolution for mesh 1

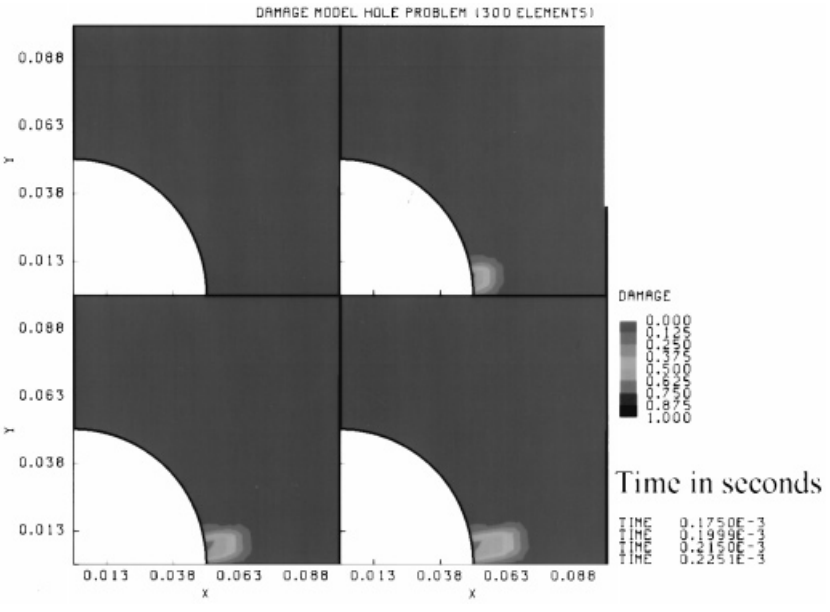

Figure 11. Damage evolution for mesh 2

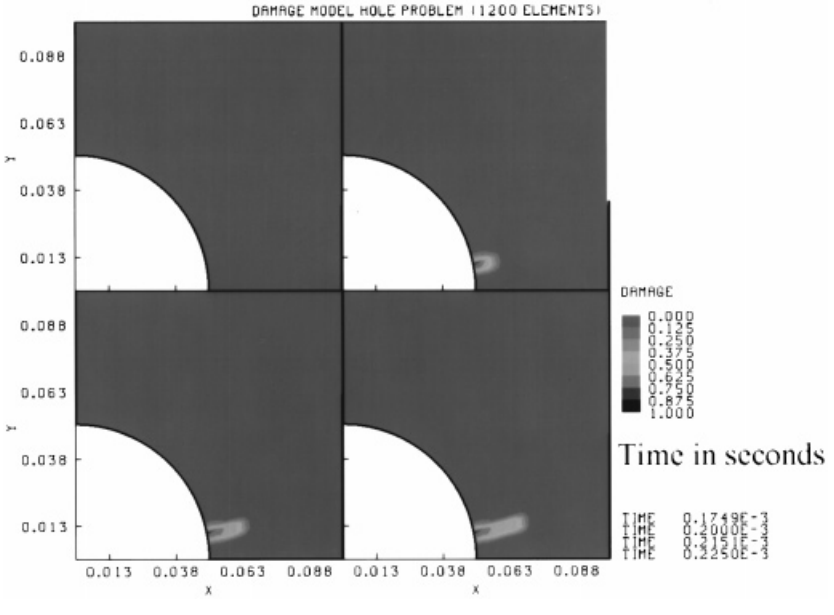

Figure 12. Damage evolution for mesh 3

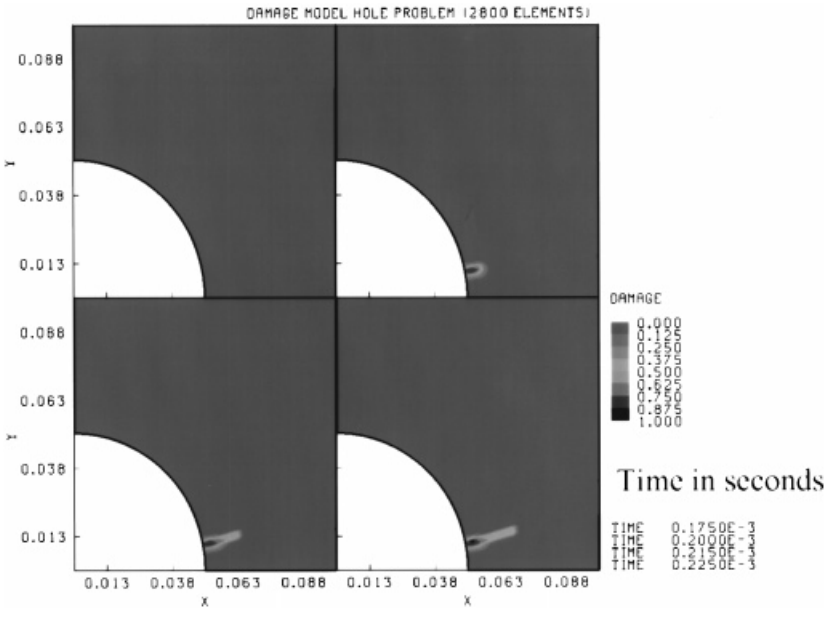

Figure 13. Damage evolution for mesh 4

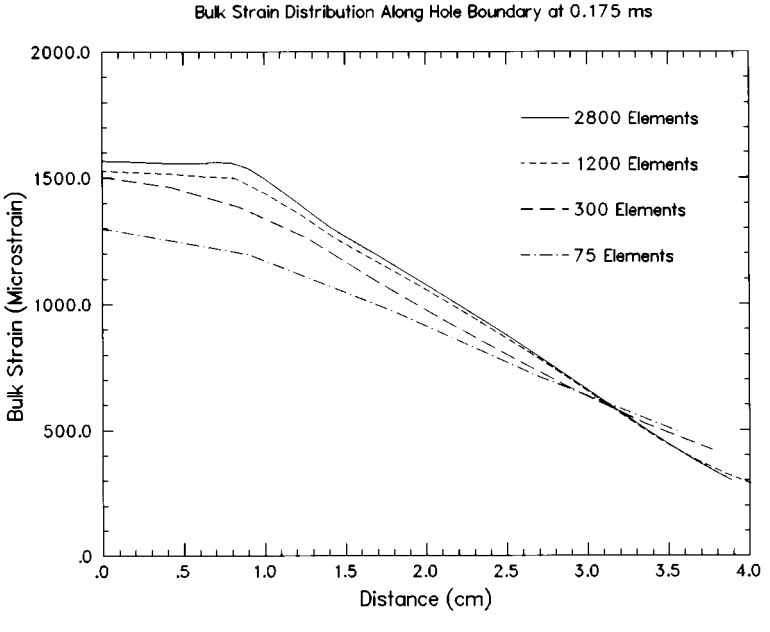

Figure 14. Bulk strain distribution at 0·175 ms

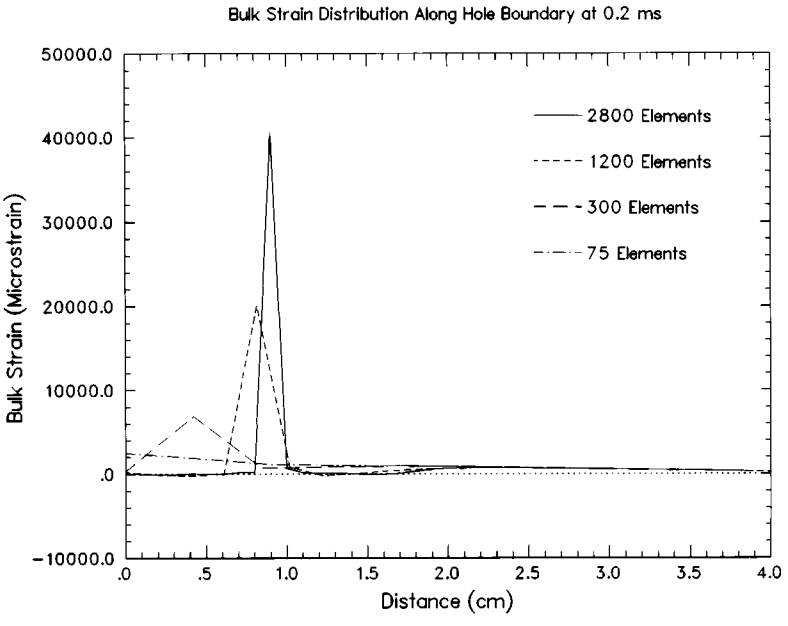

Figure 15. Bulk strain distribution at 0·2 ms

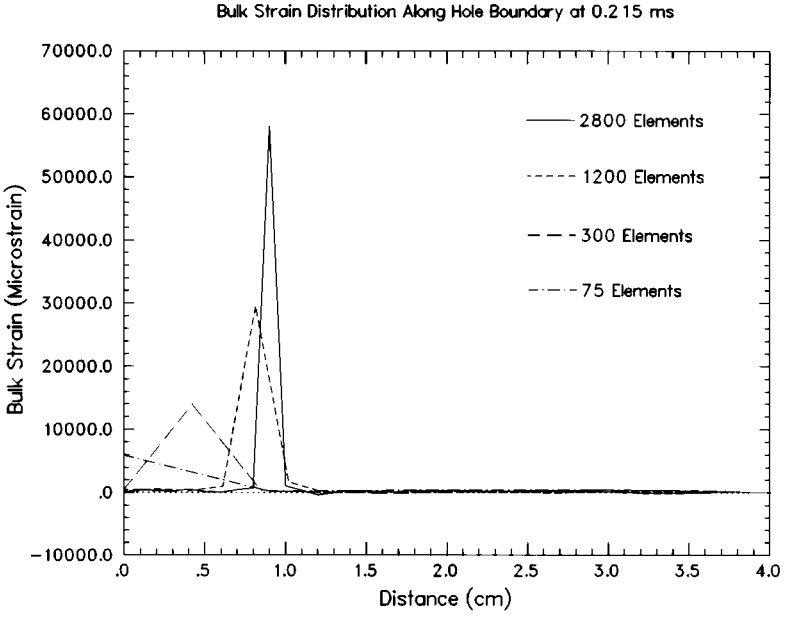

Figure 16. Bulk strain distribution at 0·215 ms

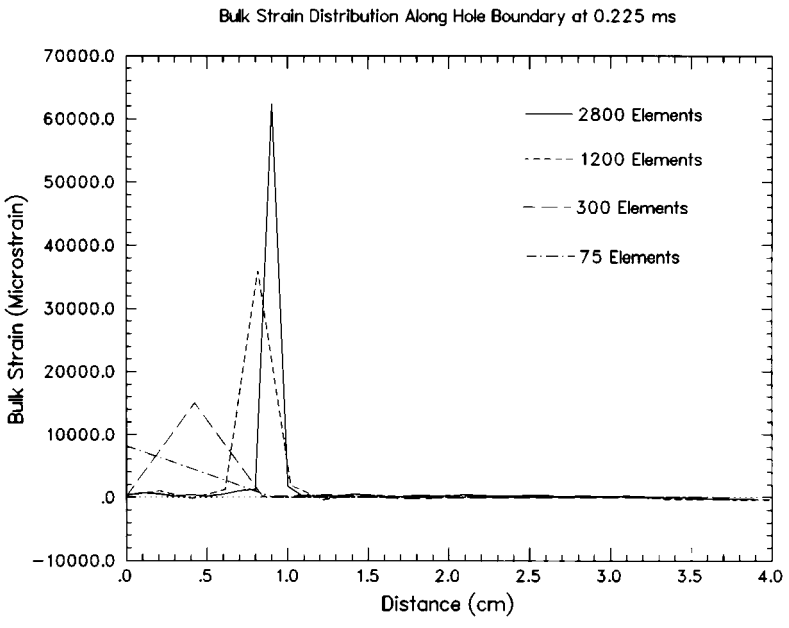

Figure 17. Bulk strain distribution at 0·225 ms

The corresponding non-local results to those in Figures 10–13 are shown in Figures 18–21. Because the characteristic length is less than the minimum dimension of mesh 1, the non-local averaging will not take effect, and the results in Figure 18 are identical to those in Figure 10. When the meshes become progressively finer, the smearing effect of the non-local results becomes more pronounced. It is observed that the narrow band of localized damage in Figure 13 is replaced by lower damage values spread over a wider area near the same location (Figure 21).

Convergence of the numerical results with mesh refinement is observed from the distribution of bulk strain along the hole boundary. Again, Figures 22–25 correspond to those in Figures 14–17. Figures. 23–25 show the convergence of bulk strain with mesh refinement. Note, however, that the magnitude of the bulk strain is much less than that for the corresponding local calculation.

SUMMARY AND DISCUSSIONS

The effect of non-local continuum formulation on the dynamic damage accumulation process in a brittle solid has been investigated. This study is based on a microcrack-based isotropic continuum damage model to illustrate the non-local effect. A non-local formulation has been added and the resulting model has been implemented into the transient dynamic finite element code PRONTO 2D for numerical computations. Characteristics of the damage model are presented. The mesh size effect has been studied through a selected example problem.

The non-local formulation introduces an additional internal length parameter which must be determined. The value of the characteristic length should be determined based on the length characterizations of material heterogeneity as well as the distance of interactions between

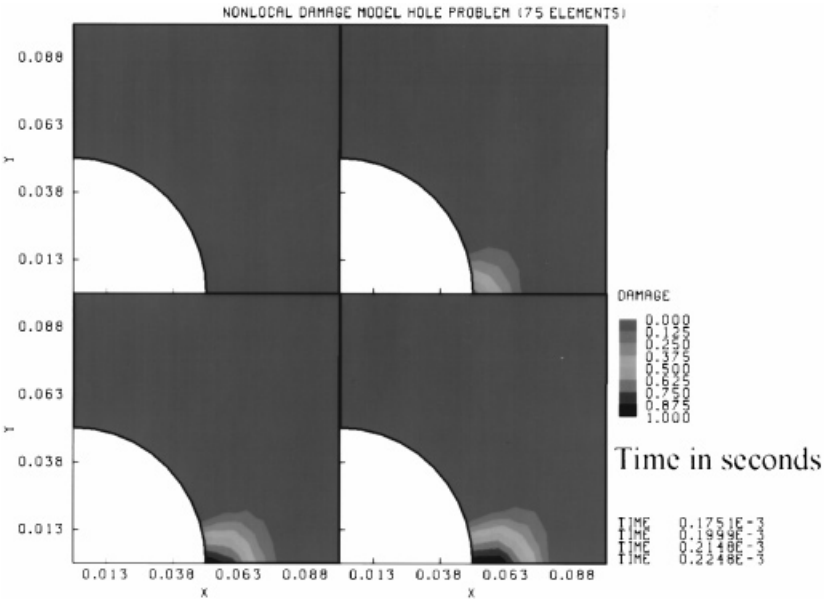

Figure 18. Non-local damage evolution for mesh 1

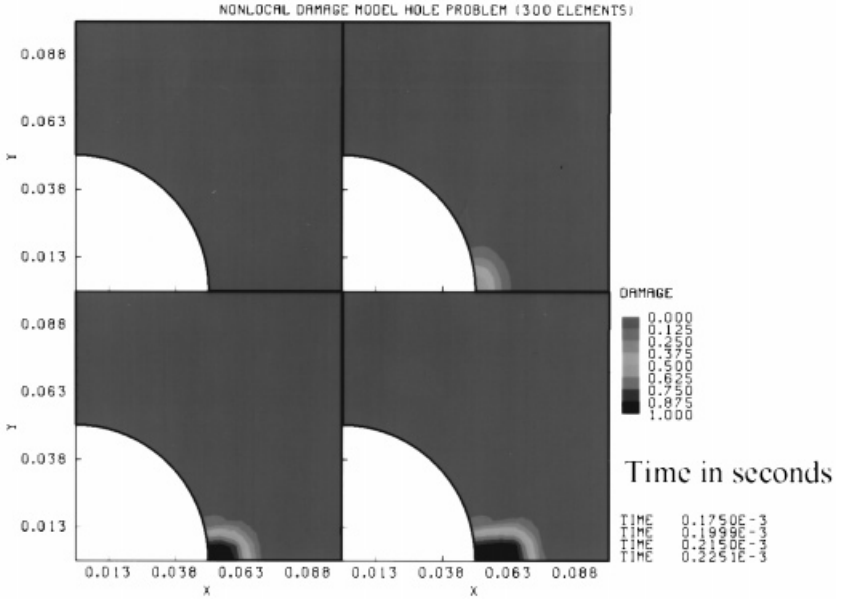

Figure 19. Non-local damage evolution for mesh 2

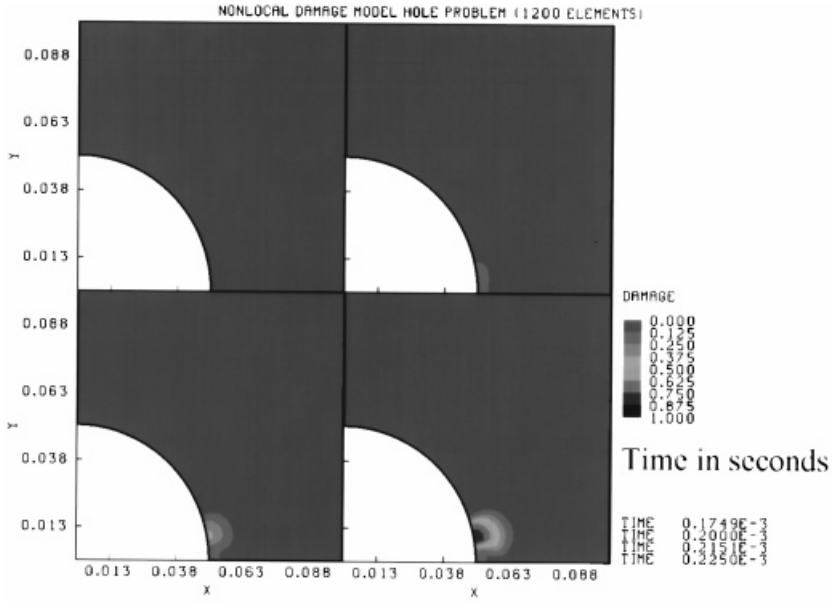

Figure 20. Non-local damage evolution for mesh 3

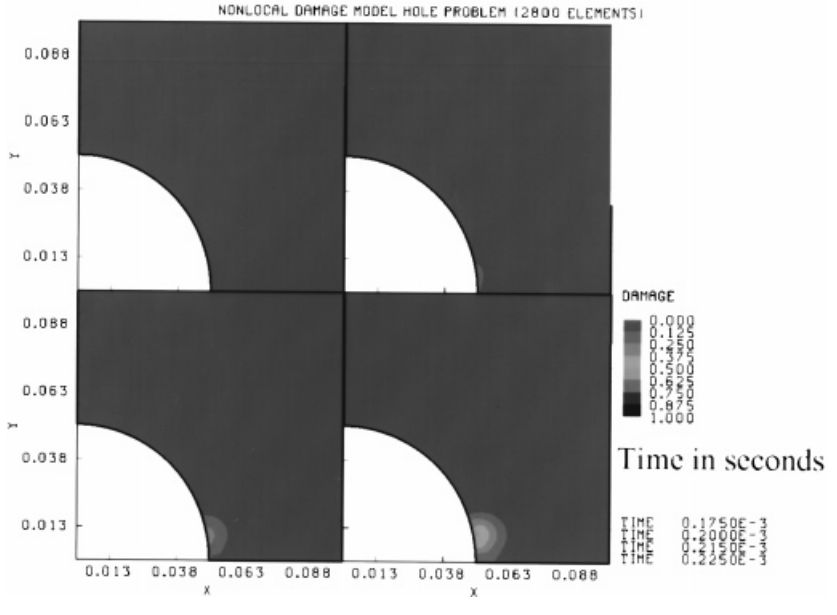

Figure 21. Non-local damage evolution for mesh 4

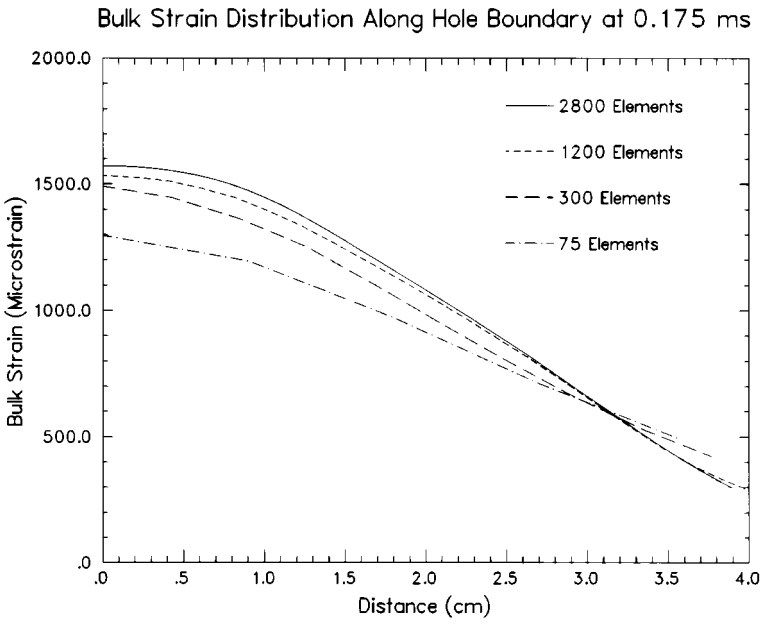

Figure 22. Non-local bulk strain distribution at 0·175 ms

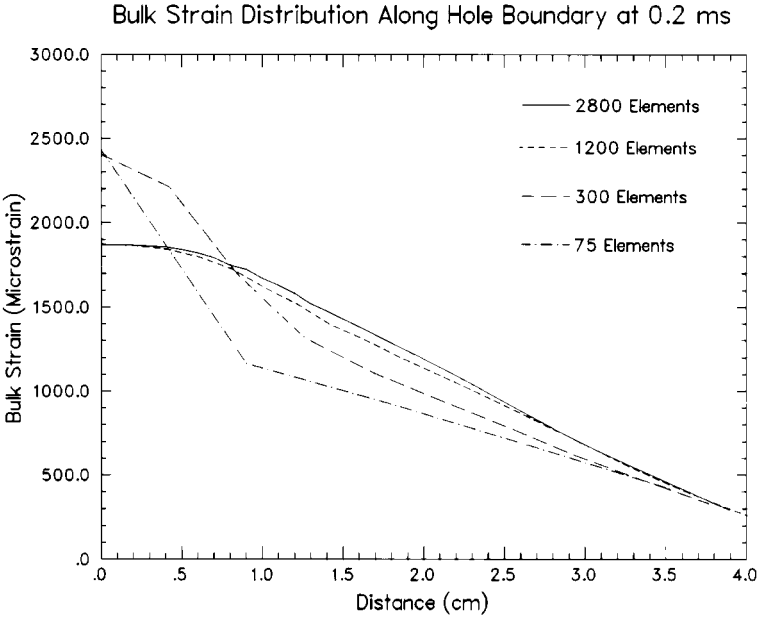

Figure 23. Non-local bulk strain distribution at 0·2 ms

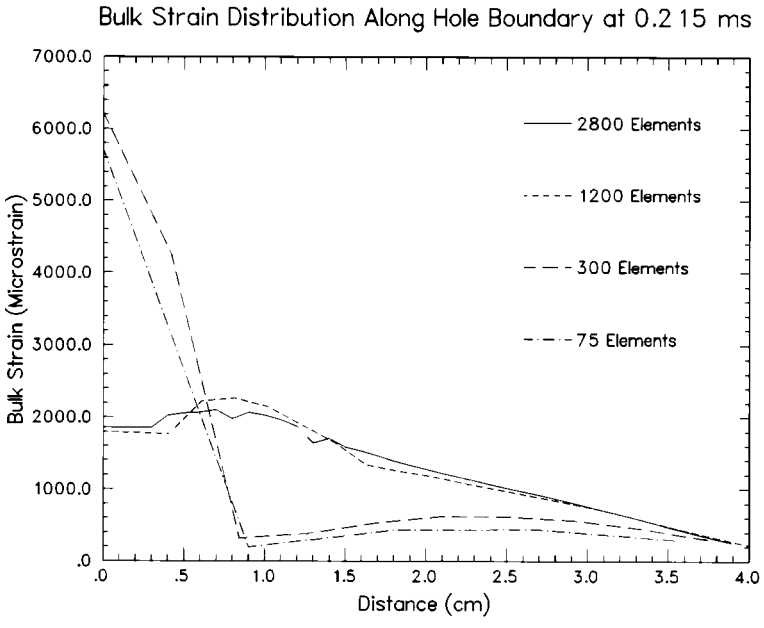

Figure 24. Non-local bulk strain distribution at 0·215 ms

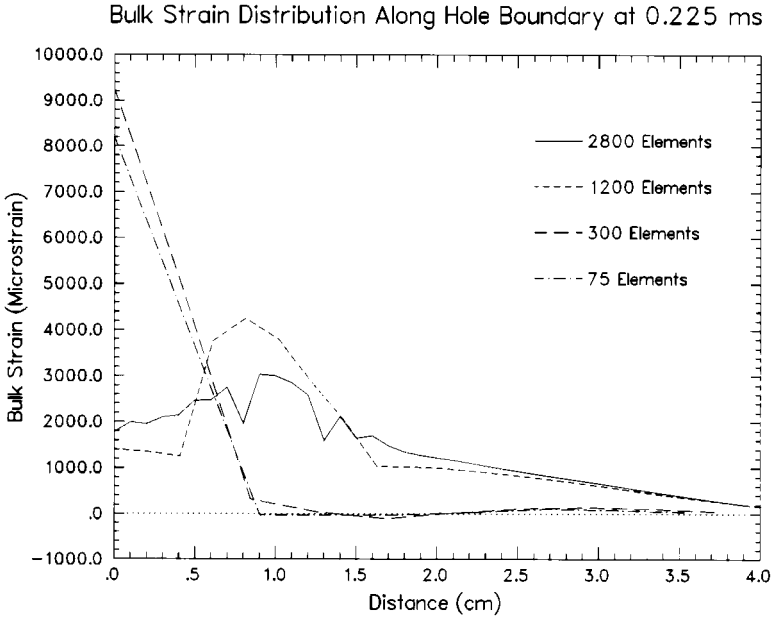

Figure 25. Non-local bulk strain distribution at 0·225 ms

microcracks. For the current damage model, this parameter was taken to be the minimum crack dimension which will be activated under the applied pulse load, *in lieu* of microstructural data. Results from the numerical simulations indicate that the non-local formulation can yield mesh-size-independent solutions. However, non-locality tends to smear out and decrease the magnitude of localized deformation patterns. In many physical situations, such as shear banding, localized and concentrated deformations are physical realities. These characteristics can potentially be lost in non-local solutions.

An additional numerical consideration is the selection of mesh size. Based on the present formulation, it is obvious that if the minimum dimension of the finite elements is larger than the characteristic internal length scale, then both local and non-local calculation will yield the same result. This is because the non-local spatial averaging is extended only to the reach of the internal length scale. Therefore, if the internal length scale can be calculated, then by selecting this length scale to coincide with the least dimension of the finite element mesh, one can use a local formulation to obtain solutions which exhibit a localized zone of correct size and the correct amount of energy dissipation. This may be the reason why many complex local continuum-based calculations, such as penetration mechanics analyses,[25] do yield reasonable solutions relative to test data.

ACKNOWLEDGEMENT

This work was funded by the Laboratory Directed Research and Development Program, Sandia National Laboratories, under the auspices of the U.S. Department of Energy under Contract Number DE-AC04-94AL85000.

REFERENCES

1. L. M. Taylor, E. P. Chen, and J. S. Kuszmaul, 'Microcrack-Induced damage accumulation in brittle rock under dynamic loading', J. Comput. Methods Appl. Mech. Eng. **55,** 301–320 (1986).
2. B. J. Thorne, 'A damage model for rock fragmentation and comparison of calculations with blasting experiments in granite', *Sandia National Laboratories Report SAND90-1389,* Albuquerque, NM, 1990.
3. B. J. Thorne, 'Application of a damage model for rock fragmentation to the straight creek mine blasting experiments', *Sandia National Laboratories Report SAND91-0867,* Albuquereque, NM, 1991.
4. E. P. Chen, 'Continuum damage mechanics studies on the dynamic fracture of concrete', in S. Mindess and S. P. Shah (eds), *Cement-Based Composites: Strain Rate Effects on Fracture*, Materials Research Society Symposia Proceedings, Vol. 64, Materials Research Society, Pittsburgh, Pa, 1986, pp. 63–77.
5. E. P. Chen and L. M. Taylor, 'Fracture of brittle rock under dynamic loading conditions', in Vol. 7, R. C. Bradt, A. G. Evans, D. P. H. Hasselman and F. F. Lange (eds) *Frature Mechanics of Ceramics*, Plenum press, New York, 1986, pp. 175–186.
6. E. P. Chen, 'Dynamic brittle material response based on a continuum damage model', in R. C. Batra, A. K. Mal and G. P. MacSithigh (eds), *Impact*, *Waves*, *and Fracture*, AMD-Vol. 205, Americal Society of Mechanical Engineers, New York, 1995, pp. 21–34.
7. E. Cosserat and F. Cosserat, *Theorie des Corps Deformables*, Herman, Paris, 1909.
8. A. C. Eringen and D. G. B. Edelen, 'On nonlocal elasticity', *Int. J. Engng. Sci*., **10,** 233–248 (1972).
9. H. B. Muhlhaus and E. C. Aifantis, 'A variational principle for gradient plasticity', *Int. J. Solids Struct*., **28,** 845–858 (1991).
10. R. de Borst and H. B. Muhlhaus, 'Gradient dependent plasticity: formulation and algorithmic aspects', *Int. J. Numer. Methods Engng*., **35,** 521–539 (1992).
11. Z. P. Bazant, 'Mechanics of distributed cracking', *Appl. Mech. Rev*., **26,** 675–705 (1986).
12. G. Pijaudier-Cabot and Z. P. Bazant, 'Nonlocal damage theory', *ASCE J. Engng. Mech*., **10,** 1512–1533 (1987).
13. Z. P. Bazant and F. B. Lin, 'Non-local yield limit degradation', *Int. J. Numeri. Methods Engng*., **35,** 1805–1823 (1988).
14. C. S. Desai and J. Toth 'Disturbed state constitutive modeling based on stress-strain and nondestructive behavior', *Int. J. Solids Struct*., **33,** 1619–1650 (1996).

15. C. S. Desai, C. Basaran and W. Zhang, 'Numerical algorithms and mesh dependence in the disturbed state concept', *Int. J. Numer.Methods Engng*., Accepted.
16. L. M. Taylor and D. P. Flanagan, 'PRONTO 2D — a two dimensional transient solid dynamics program', *Sandia National Laboratories Report SAND86-0594,* Albuquerque, NM, 1987.
17. B. Budiansky and R. J. O'Connell, 'Elastic moduli of a cracked solid', *Int. J. Solids Struct*., **12,** 81–97 (1976).
18. D. E. Grady and M. E. Kipp, 'Continuum modeling of explosive fracture in oil shale', *Int. J. Rock Mech. Mining Sci*., **17,** 147–157 (1980).
19. D. E. Grady, 'The mechanics of fracture under high-rate stress loading', in Z. P. Bazant (ed.), *Preprints of the William Prager Symp. on Mechanics of Geomaterials*: *Rocks*, *Concrete and soils*, Northwestern University, Evanston, Ill, 1980, pp. 149–188.
20. R. Englman and Z. Jaeger 'Theoretical aids for the improvement of blasting efficiencies in Oil shale and rocks', *AP-TR-12/87,* Soreq Nuclear Research Center, Yavne, Israel, 1987.
21. D. C. Drucker and W. Prager, 'Soil mechanics and plastic analysis or limit design', *Quart. Appl. Math*., **10,** 157–165 (1952).
22. M. E. Kipp, D. E. Grady and E. P. Chen, 'Strain-rate dependent fracture initiation', *Int. J. Fracture*, **16,** 471–478 (1980).
23. M. E. Kipp and D. E. Grady, 'Numerical studies of rock fragmentation', *Sandia National Laboratories Report SAND79-1582,* Albuquerque, NM, 1978.
24. R. de Borst, L. J. Sluys, H. B. Muhlhaus and J. Pamin, 'Fundamental issues in finite element analyses of localization of deformation', *Engng. Comput*., **10,** 99–121 (1993).
25. E. P. Chen, 'Simulation of concrete perforation based on a continuum damage model', in A. Carpinteri (ed.), *Size-Scale Effects in the Failure Mechanisms of Materials and Structures*, E & FN SPON, An imprint of Chapman & Hall, New York, 1996, pp. 574–587.

